BIAXIAL STRETCHING OF PET FILMS: A MOLECULAR DESCRIPTION

Jean-François Tassin*[1], Murielle Vigny[1], Didier Veyrat[2]

[1] Chimie et Physique des Matériaux Polymeres, UMR 6515, Université du Maine, Avenue Olivier Messiaen, 72085 Le Mans Cedex 9, France

[2] Toray Plastics Europe, Saint Maurice de Beynost, BP 140, 01701 Miribel Cedex, France

SUMMARY: Biaxially oriented poly(ethylene terephthalate) films were prepared under well defined stretching conditions in order to mimic the three stages of the industrial inverse drawing process. Molecular orientation has been characterized through X-ray diffraction and infrared dichroism. The main orientation mechanisms in the constant-speed drawing of an amorphous film as well as in the constant-force transverse drawing of monodrawn samples are described. It is shown that relaxation phenomena dominate the orientation of an amorphous sample. Reorientation along the second drawing direction involves rotation of crystalline blocks along the draw direction and further crystalline growth. The high-temperature heating stage leads to an almost four-fold increase in the size of the crystallites. The orientation of the amorphous phase is controlled by the mechanisms occurring during crystallization (relaxation followed by extension).

INTRODUCTION

Thanks to its economic importance and relatively easy processing conditions, the behavior of poly(ethylene terephthalate) (PET) films under various types of deformation has been the subject of numerous studies in the past[1-29]. They were mainly devoted to characterization of molecular orientation, mechanical properties and end-use properties such as gas permeability. It is clearly established that mechanical properties of the final films are mainly controlled by their structure at molecular level, originating from various thermal and deformation conditions experienced by the film throughout its production process. It is therefore of great interest to be able to afford an accurate characterization of molecular orientation and structure in oriented samples.

 CCC 1022-1360/99/$ 17.50+.50/0

In most of the studies, uniaxially or constant-width-drawn samples obtained from amorphous unoriented films were considered. Less studies report on the structure of biaxially stretched films, probably due to the difficulties in obtaining films with well defined deformation conditions and in clean characterization of samples that have lost the uniaxial symmetry.

It was therefore stimulating to carry out accurate characterizations of biaxially oriented PET films that closely follow the industrial processing conditions. However, due to geometric factors in industrial processes, it is almost impossible to pick, from the production or pilot lines, films spanning over a wide range of conditions in order to extract from the data the influence of parameters, such as draw ratio, rate and temperature. Nevertheless, films can be taken at specific positions in the line. This allowed us to produce, on a laboratory scale, model films that are stretched under very well defined procedures and conditions. This method has been used to follow the development of molecular orientation and structure in the normal stretching process of PET films. In this paper, we will present the main lines of the events occurring during the inverse sequence.

In these processes, the molten PET film extruded through a flat die is quenched on a cold roll, leading to a rather thick amorphous film. It is first stretched transversally to the machine direction thanks to a series of clamps on each side of the film. During this stage, the deformation kinetics is set by the rate and the profile on which the clamps are moving. The stretching temperature is slightly above the glass transition temperature, in the range 90 - 120 °C. The transversally monodrawn film is then stretched between rolls along the machine direction. In this case, the draw ratio is determined by the ratio of the speeds of the slow and fast rolls, but the drawing is carried out at a constant force in such a way that the kinetics depends on the temperature conditions and on the state of orientation of the monodrawn films. The stretching temperature is in the range 100-140 °C. Finally, the biaxially stretched film undergoes a heat setting treatment at temperatures slightly below the melting temperature of PET crystals.

Hence, there are three main steps in this process, which have been studied using model samples. The present paper is divided into four sections. In the first one, information on the ways the model samples have been obtained is given with a brief description of characterization techniques. In each following section, the development of molecular orientation occurring at each stage of the process will be described, and a brief comparison will be given with the normal stretching sequence, in which the two stretching steps are inverted.

SAMPLES AND CHARACTERIZATION TECHNIQUES

Production of model samples

As quoted above, the first stretching process is carried out at a constant drawing speed. It is, however, not strictly uniaxial since the other dimension in the plane of the film is kept constant. Amorphous unoriented PET films provided by Rhône-Poulenc Films were used as starting materials. The molecular weight determined from intrinsic viscosity measurements was 39000. Films were cut into rectangular pieces with a width of 100 mm and a length of 30 mm. They were stretched on a special stretching machine designed in the Saint Fons Research Center of Rhône-Poulenc. The sample was first preheated for 30 s at the stretching temperature and stretched at a nominal drawing speed of 0.75 s^{-1} (close to the industrial process conditions) up to a programmed draw ratio. Typical stretching temperatures ranged from 85 to 115 °C. The film was kept at constant width during stretching with the aid of two small clamps on each side. Finally, the sample was quenched with blown air at room temperature. The effective draw ratio was determined using a grid drawn on the sample.

For the second step, model samples were obtained using a transversally monodrawn film, taken from a pilot line (Rhône-Poulenc Films), as starting material (draw ratio 4, draw temperature 91 °C). Again, rectangular pieces were cut, brought to the desired temperature during 10 s (sufficient to ensure thermal stabilization and avoid a too large change in the state of orientation and in the structure of the film), and stretched with a constant drawing force. Three different stretching temperatures (105, 115, 125 °C) and three applied loads (15, 20, 25 MPa) were used. In this type of stretching, the deformation kinetics is dependent on temperature and the applied load. Description is given below, where it is shown that various types of samples can be obtained.

Finally, the thermosetting step was studied using a biaxially oriented film taken at the end of the longitudinal drawing in a pilot line (draw ratios 4x4). 100 x 100 mm pieces were cut from this film, glued inside a thick cardboard frame in order to avoid any retraction during the heat setting experiment. The samples were first preheated at a temperature of 100 °C during 5 s and then subjected to an annealing treatment at a fixed temperature (200 °C) for a given time (3 - 20 s). The samples were finally cooled with blown air at room temperature.

Definition of axes and orientation

In this paper, we choose X_1 as the transverse (i.e., the first drawing) direction, X_2 as the machine direction (second drawing direction) and X_3 as the direction normal to the plane of the film. Hereinafter, the orientation of any molecular direction u with respect to any

macroscopic direction X_i will be quantified by the average value of the second-order Legendre polynomial[30]:

$$P_{200}^{u/X_i} = 0.5\,(3\cos^2\theta_{u,Xi} - 1)$$

where $\theta_{u,Xi}$ is the angle between the axes u and X_i and the brackets denote an average over all the molecular units.

Experimental techniques for orientation characterization

Refractive indices

The refractive indices were measured along the three main directions of film using an Abbe refractometer. They were used to calculate the overall orientation of the normal to the benzene ring averaged over the crystalline and amorphous phases, using expressions given in ref.[26]. The average refractive index was also used to calculate the density and crystallinity of our samples.

X-ray diffraction

Wide-angle X-ray diffraction has been used to characterize the crystalline morphology as well as the orientation of two crystallographic directions. The two reflections investigated are $(\bar{1}05)$, whose plane normal is close to the chain axis direction, and (100), whose plane normal is close to the normal to the benzene ring. The procedure used to collect the diffracted intensity and to compute the order parameter P_{200} of these two directions with respect to the principal directions of the sample is accurately described elsewhere[27].

The angular broadening of the diffraction peaks associated with the directions $(\bar{1}05)$, (010) and (100) was used to estimate the dimensions of the crystallites using the Sherrer formula. These dimensions will be referred as the length, width and thickness of the crystallites, respectively.

Infrared dichroism

Polarized IR spectra of the samples were taken on a Bomen Ramspec FTIR spectrometer using normal incidence and 45°-tilted film experiments. After deconvolution of the spectrum between 825-1060 cm^{-1} into 22 vibration bands, attention was given to the 1018 cm^{-1} absorbance which is associated with an in-plane vibration of the benzene ring with a transition moment parallel to the C_1-C_4 axis. The same method as in previous studies[5,24,27,31,32] was applied to calculate the orientation of the C_1-C_4 axis averaged over the crystalline and amorphous phase with respect to the principal directions of the film.

CONSTANT-SPEED STRETCHING OF AMORPHOUS FILMS

Since many studies in the literature are focused on this type of stretching, only its main features will be described. The major event in this stretching of an amorphous film slightly above the glass transition temperature is the appearance of orientation-induced crystallization during stretching. As an illustration, Fig. 1 shows the evolution of the crystallinity with respect to the draw ratio at various temperatures. At the highest temperature, where samples could be obtained in a sufficiently large range of draw ratios, the crystallinity shows a usual sigmoidal shape. It can be seen that crystallization appears at lower draw ratios as temperature decreases, in agreement with previous studies[4,8,10,11].

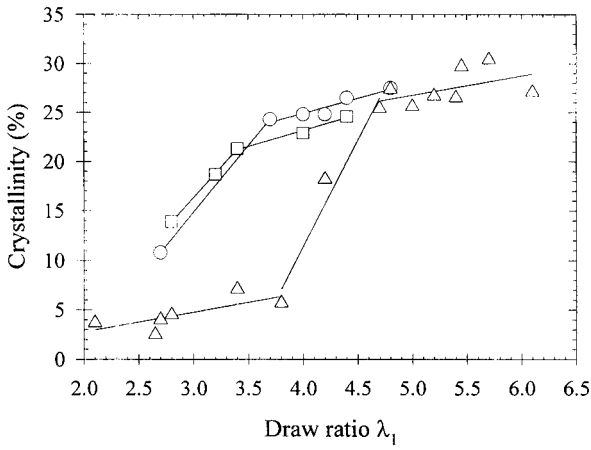

Figure 1. Crystallinity versus effective draw ratio (□ T = 95 °C; o T = 105 °C; Δ T= 115 °C)

The orientation of the chain axes (more precisely, $(\bar{1}05)$ plane normals) with respect to the stretching direction is given in Fig. 2. The chain axes appear to align more and more towards the draw direction as the draw ratio increases or the temperature decreases. Figure 2 shows the importance of relaxation phenomena, even for crystalline orientation, since decrease in orientation with temperature cannot be solely explained by the shift in the appearance of orientation-induced crystallization.

Calculation of $P_{200}^{[T05]/\chi 3}$ yields value of -0.45 indicates that the chain axes almost lie in the plane of the film, clearly showing the non-uniaxial orientation of the sample.

Interestingly, the orientation behavior of the material during stretching can be understood using the concept of a molecular network, especially after appearance of crystallization. Indeed, we have shown previously[33] that the large increase in the stress measured after a

plateau, where crystallization occurs, can be explained by the extension of the part of chains trapped between crystalline blocks.

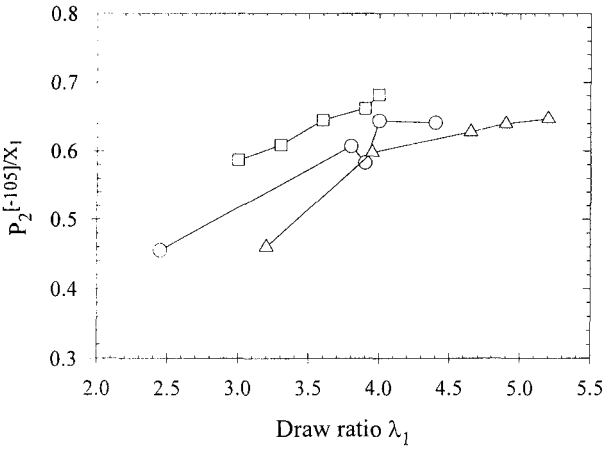

Figure 2. Orientation of the (-105) plane normals with respect to X_1 versus the draw ratio (□ T = 95 °C; ○ T = 105 °C; Δ T = 115 °C)

This is qualitatively confirmed by the behavior of the orientation in the amorphous phase which shows a significant increase after crystallization. Essentially, two types of networks are observed. At temperatures below 105 °C, quantitative examination of stress-strain curves yields a modulus of 8 MPa instead of only 3.4 MPa at 115 °C. A looser network is thus obtained at higher temperatures. It can be thought that both chain entanglements and crystallites act at low temperatures whereas only the latter play a significant role at higher ones.

The existence of these two types of networks has also been observed in constant-force drawings[26]. However, in this type of stretchings, a higher orientation of chain axes is observed and the orientation in the crystalline phase is entirely controlled by the draw ratio[23].

CONSTANT-FORCE STRETCHING OF MONODRAWN SAMPLES

Stretching kinetics

This stretching is characterized by an unusual kinetics, a typical example of which is given in Fig. 3. The stretching process starts with low strain rates. A maximum is observed and finally, at longer times, the stretching process stops showing that a maximum (and equilibrium) value of the draw ratio is obtained for a given condition of temperature and the applied load. This behavior is completely similar to the deformation of amorphous samples in the same type of stretching. It can be noted that high strain rates (a few s^{-1}) are obtained.

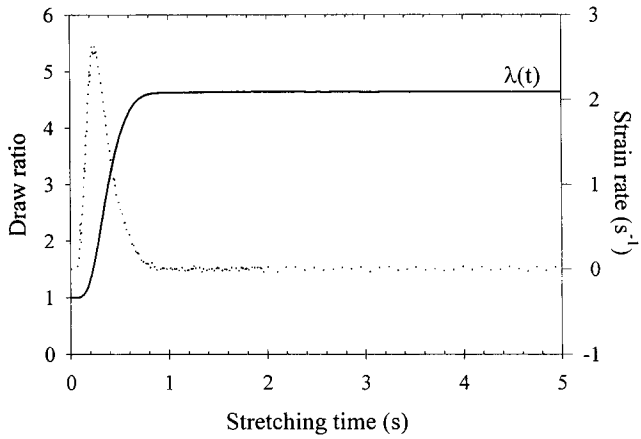

Figure 3. Stretching kinetics under constant force (T = 115 °C, engineering stress 20 MPa).

Films with a draw ratio lower than the plateau value can be simply obtained by stopping mechanically the deformation before it reaches the plateau value. We refer to them as "quenched samples". Their study affords interesting information about the deformation mechanisms.

Both the growing temperature and growing applied load increase the deformation kinetics and the equilibrium deformation. However, the influence of the applied load is the most pronounced.

Orientation measurements

An important feature of this second stretching is that the reorganization of the structure is carried out at a constant crystallinity. The evolution of the orientation of the chain axes with respect to the three directions of the film is given in Fig. 4.

The chain axes remain oriented in the plane of the film as the deformation proceeds. Their orientation, which was originally along X_1, gradually moves along X_2. Quantitatively, the orientation along X_2 is less than the previous one along X_1, although the draw ratio is higher. Nevertheless, the reorganization mechanisms appear very efficient since moderate draw ratios (of the order of 2.2) are sufficient to create a biaxially equilibrated orientation (in terms of P_{200}).

The calculation of P_{200} from X-ray data is, however, somewhat hiding the details of the molecular processes occurring in the crystalline phase. Figure 5 shows the diffracted intensity (in the plane of the film) versus the considered direction in this plane, for various draw ratios.

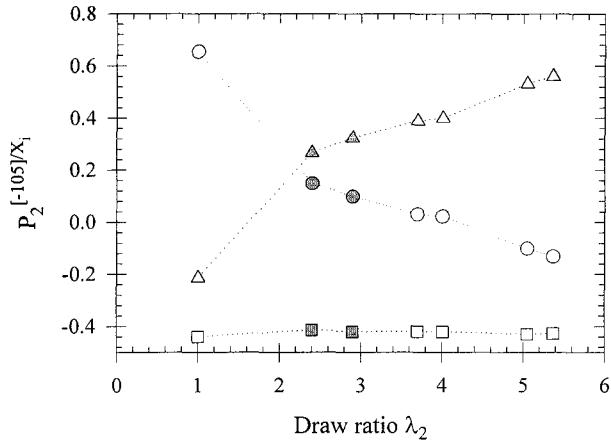

Figure 4. Orientation of the chain axes in the crystalline phase versus the draw ratio (T = 125 °C; grey symbols are quenched samples; □ X_3; Δ X_2, O X_1).

As the draw ratio increases, the measured intensity towards X_1 decreases rapidly. Even at moderate draw ratios, the crystals initially oriented along X_1 have almost disappeared. At the same time, an increase in intensity is observed along X_2 and a significant part of the crystalline chain axes are lying at intermediate directions between X_1 and X_2. A relative maximum is detected at intermediate angles. These results point to a mechanism where crystals rotate during deformation.

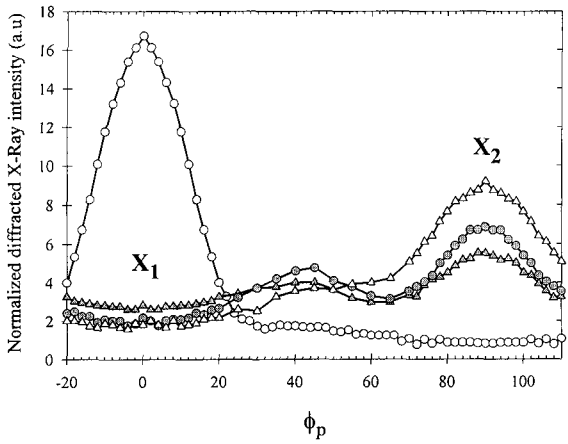

Figure 5. Distribution of diffracted intensity in the plane of the film (draw ratios: O 1; grey O 2.4; grey Δ 2.9; Δ 3.7)

The measurement of the crystal length as a function of their position, plotted in Fig. 6, corroborates this assumption. Even at small draw ratios, the length of the crystals lying around the intermediate maximum is important (but less than the initial one) and X_2-oriented crystals show a size which becomes rapidly higher than that of those initially oriented along X_1. The length of the crystals oriented along X_2 increases with the draw ratio, meaning that drawing

favors the growth of these crystals at the expense of those lying at intermediate angles (since the transformation is carried out at an almost constant crystallinity).

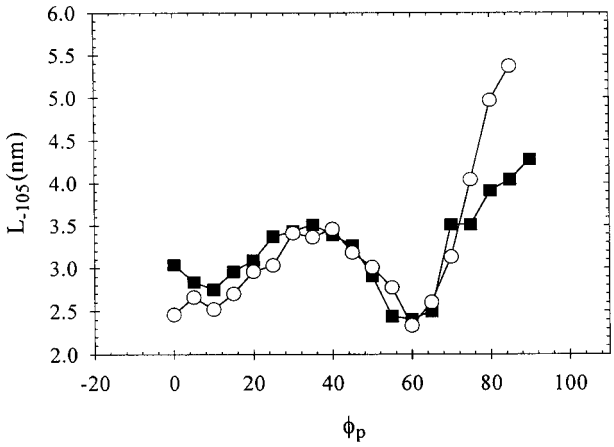

Figure 6. Length of the crystals versus their position in the plane of the film (draw ratios: ■ 2.4; o 2.7)

This mechanism is totally different from that observed with a constant speed drawing of monodrawn samples, where rotation of small crystals was present but not being the major phenomenon[27,28].

HIGH-TEMPERATURE ANNEALING: INFLUENCE OF ANNEALING TIME

The main event of this high-temperature annealing process (200 °C) is the important growth of the crystals along the three investigated directions. The volume of the crystals (roughly estimated as the product of their size along the three directions) is plotted versus the annealing time in Fig. 7.

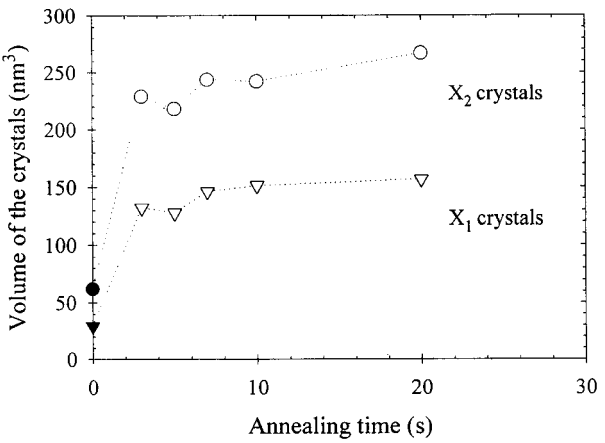

Figure 7. Volume of the crystals versus annealing time at 200 °C (o X_2 crystals, ∇ X_1 crystals)

A four-fold increase in the volume is observed. Interestingly, a small number of crystals remaining oriented along X_1 also experiences an increase in their dimensions. Since the sample is not deformed during this stage, the driving force for the orientation and structural changes is not as simple as above. Our analysis is based on the fact that the increase in size (and possibly in the number) of the crystals is the driving force.

The strong increase in crystallinity appears clearly in Fig. 8 where the diffracted intensity in the plane of the film is plotted versus the direction for various annealing times. Short annealing times lead to a pronounced increase in the number of crystals lying along X_2. Longer times favor an increase in intensity mainly along X_1, but to a lesser extent.

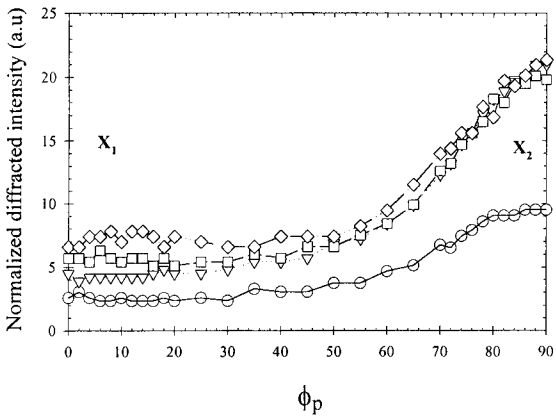

Figure 8. Diffracted intensity in the plane of the film for various annealing times: O 0, ∇ 3 s, □ 7 s, ◊ 20 s

As far as the orientation is concerned, an increase in the orientation along X_2 is expected at short times, followed by a decrease at longer ones. The values are plotted in Fig. 9 versus the annealing time. In order to get information about the mechanisms involved in the amorphous phase, we have plotted the evolution of the orientation of the C_1-C_4 axes of the benzene ring versus the annealing time in Fig. 10.

Obviously, Fig. 10 represents the behavior of both the crystalline and amorphous phases. Short times are characterized by a decrease in average orientation along X_2, whereas an increase was observed for the crystalline phase alone. This shows unambiguously that amorphous orientation relaxes at short times. The growth of the length of the X_2-oriented crystals is responsible for this behavior. At longer times, an increase in average orientation along X_2 is observed whereas, at the same time, the crystalline orientation decreases. This points to an increase of orientation of amorphous segments along X_2, without any stretching.

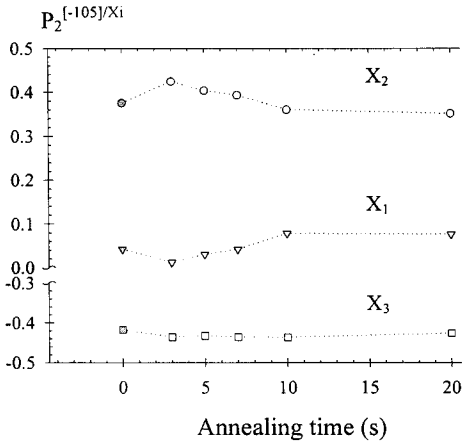

Figure 9. Orientation of chain axes in the crystalline phase versus annealing time at 200 °C (∇X_1, $O X_2$, $\square X_3$)

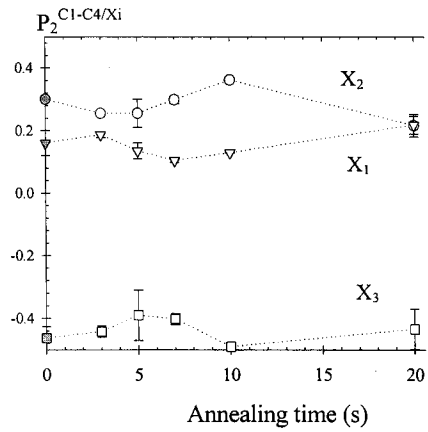

Figure 10. Orientation of the C_1-C_4 axes averaged over the crystalline and amorphous phases versus annealing time at 200 °C (∇X_1, $O X_2$, $\square X_3$)

A possible way in which amorphous segments can be stretched is through the lateral growth of the crystals involving the formation of folds at the surfaces. In this mechanism, gauche conformations, instead of being located statistically in the amorphous phase, are concentrated at crystal surfaces, inducing stretching of amorphous chains.

We therefore see that complex mechanisms occur in the amorphous phase, which are driven by important changes in the size of the crystals.

CONCLUSIONS

In this paper, we have summed up the main events occurring, at a molecular level, during the inverse sequence of the biaxial stretching process of PET films. We have shown that although the draw ratios are rather similar in the normal or in the inverse sequence, the state of orientation and the deformation mechanisms can be very different. This is a consequence of the completely different deformation kinetics which appear either in a constant-speed drawing or in a constant-force drawing, emphasizing the role of relaxation phenomena.

REFERENCES

1. A. Cunningham, G.R. Davies, I.M. Ward *Polymer*, **15**, 743 (1974)
2. A. Cunningham, I.M. Ward, H.A. Willis, V. Zichy *Polymer*, **15**, 749 (1974)
3. N. Yoshihara, A. Fukushima, Y. Watanabe, A. Nakai, S. Nomura, H. Kawai *J. Soc. Fiber Sci. Technol. (Jpn.)*, **37**, T-387 (1981)
4. S.R. Padibjo, I.M. Ward *Polymer*, **24**, 1103 (1983)
5. M. Cakmak, J. Spruiell, L. White, J.S. Lin *Polym. Eng. Sci.*, **27**, 893 (1987)

6. M. Cakmak, J.L. White, J.E. Spruiell *Polym. Eng. Sci.*, **29**, 1534 (1989)
7. B. Clauss, D.R. Salem *Polymer*, **33**, 3193 (1992)
8. D.R. Salem *Polymer*, **33**, 3182 (1992)
9. D.R. Salem *Polymer*, **33**, 3189 (1992)
10. D.R. Salem *Polymer*, **35**, 771 (1994)
11. G. Lebourvellec, L. Monnerie, J.P. Jarry *Polymer*, **27**, 856 (1986)
12. G. Lebourvellec, L. Monnerie, J.P. Jarry *Polymer*, **28**, 1712 (1987)
13. G. Lebourvellec, J. Beautemps, J. Jarry *J. Appl. Polym. Sci.*, **39**, 319 (1990)
14. G. Lebourvellec, J. Beautemps *J. Appl. Polym. Sci.*, **39**, 329 (1990)
15. A. Ajji, K.C. Cole, M.M. Dumoulin *Polymer*, **36**, 4023 (1995)
16. A. Ajji, J. Guevremont, K.C. Cole, M.M. Dumoulin *Polymer*, **37**, 3707 (1996)
17. P. Chandran, S. Jabarin *Adv. Polym. Technol.*, **12**, 119 (1993)
18. P. Chandran, S. Jabarin *Adv. Polym. Technol.*, **12**, 133 (1993)
19. P. Chandran, S. Jabarin *Adv. Polym. Technol.*, **12**, 153 (1993)
20. R.M. Gohil, D.R. Salem *J. Appl. Polym. Sci.*, **47**, 1989 (1993)
21. R.M. Gohil *J. Appl. Polym. Sci.*, **48**, 1635 (1993)
22. R.M. Gohil *J. Appl. Polym. Sci.*, **48**, 1649 (1993)
23. P. Lapersonne, J.F. Tassin, L. Monnerie, J. Beautemps *Polymer*, **32**, 3331 (1991)
24. P. Lapersonne, D.I. Bower, I.M. Ward *Polymer*, **33**, 1266 (1992)
25. P. Lapersonne, D.I. Bower, I.M. Ward *Polymer*, **33**, 1277 (1992)
26. P. Lapersonne, J.F. Tassin, L. Monnerie *Polymer*, **35**, 2192 (1994)
27. J.B. Faisant de Champchesnel, D.I. Bower, I.M. Ward, J.F. Tassin, G. Lorentz *Polymer*, **34**, 3763 (1993)
28. J.B. Faisant de Champchesnel, J.F. Tassin, D.I. Bower, I.M. Ward, G. Lorentz *Polymer*, **35**, 4092 (1994)
29. J.B. Faisant de Champchesnel, J.F. Tassin, L. Monnerie, P. Sergot, G. Lorentz *Polymer*, **38**, 4165 (1997)
30. I.M. Ward *Adv. Polym. Sci.*, **66**, 81 (1985)
31. D.A. Jarvis, I.J. Hutchinson, D.I. Bower, I.M. Ward *Polymer*, **21**, 41 (1980)
32. I.J. Hutchinson, I.M. Ward, H.A. Willis, V. Zichy *Polymer*, **21**, 55 (1980)
33. M. Vigny, J. F. Tassin, A. Gibaud, G. Lorentz *Polym. Eng. Sci.*, **37**, 1785 (1997)